Computational Materials Science 206 (2022) 111277

Contents lists available at ScienceDirect

Computational Materials Science

journal homepage: www.elsevier.com/locate/commatsci

The mechanical property and micro-mechanism of nanoparticle-contained graphene foam materials under uniaxial tension

Muhammad Bilal Khan [a,c], Chao Wang [b,d,*], Shuai Wang [e], Shaohua Chen [a,c,*]

[a] Institute of Advanced Structure Technology, Beijing Institute of Technology, Beijing 100081, China
[b] LNM, Institute of Mechanics, Chinese Academy of Sciences, Beijing 100190, China
[c] Beijing Key Laboratory of Lightweight Multi-functional Composite Materials and Structures, Beijing Institute of Technology, Beijing 100081, China
[d] School of Engineering Science, University of Chinese Academy of Sciences, Beijing 100049, China
[e] College of Mechanical and Electrical Engineering, Beijing University of Chemical Technology, Beijing 100029, China

ARTICLE INFO

Keywords:
Nanoparticles
Graphene foam
Uniaxal tension
Mechanical property
Micro-mechanism
Coarse-grained molecular dynamics

ABSTRACT

Nanoparticle-contained graphene foams (NP-GrFs) have been widely concerned and used in many practical applications in recent years. However, the mechanical property and its micro-mechanism of such a new composite material are still poorly understood. In this work, a coarse-grained NP-GrFs model is established to systematically study the mechanical response of NP-GrFs under uniaxial tension as well as the size and volume fraction effects of nanoparticles. It is found that both the initial modulus and tensile strength depend on the size and volume fraction of NPs, both of which can increase by almost an order of magnitude. Furthermore, when the volume fraction of nanoparticles increases, the strain hardening phenomenon occurs. Two main enhancing mechanisms are found. One is the increased adhesion between neighbor sheets by NPs and the other is the homogenized stress due to the extrusion of NPs. The present results should be useful not only for understanding the microstructure-determined mechanical properties of NP-GrFs but also for the design of advanced functional materials or devices based on GrFs.

1. Introduction

Graphene foam(GrF), as a typical carbon-based nanoporous material, owns a flexible density range [1,2], extraordinary compressibility [3], high chemical and thermal stability [4], good energy adsorption capacity [5] and tunable specific area [6], etc. All these properties make GrFs eligible not only for conventional applications, such as energy adsorption [5], environment purification [7] and composite materials [8] but also for cutting-edge applications like biocompatible scaffold [9] and batteries [10–12].

In most practical applications, various nano-particles (NPs) are often intentionally embedded in the porous structure of GrFs to enable specific functions. For example, the metal oxide nanoparticles (NPs) of Fe_3O_4 [13], CoO [14] and SnO_2 [15] are often filled in GrFs as an alternative anode material to enhance the electrochemical lithium storage performance. GrFs added respectively with 59, 67, 39 and 46 wt% of Pd, Pt, Ni and Sn NPs could greatly improve the sensing performance of hydrogen gas [16–18]. As a flexible electronic device [19], Fe_3O_4 magnetic NP-embedded GrFs could achieve up to 52% reversible magnetic field-induced strain and strain-dependent electrical resistance. More examples about the NP-GrFs are given in Table S1 in Supporting Materials. In these studies, the physical/chemical functions inherited from NPs were mainly concerned, but the mechanical properties are rarely involved. However, as a functional material or device, the mechanical property of NP-GrFs should be equally important when the material or device is in service, for an example, the large deformation in flexible electronic devices prepared from GrF embedded Fe_3O_4 NPs [19].

Fortunately, the mechanical properties [4,20–33], physical properties [4,34,35] and the microscopic mechanisms of pure GrF materials have been comprehensively studied in recent years. For examples, Agarwal et al. [36] performed the in-situ tensile test on GrFs with the scanning electron microscopes (SEM) and found that the tensile elastic modulus is 69.9 GPa, four orders of magnitude higher than 1.2–1.5 MPa under compression. The first full-atomic molecular dynamics (FAMD) simulation was carried out by Baimova et al. [37] to investigate the shear deformation and hydrostatic compression behavior of GrFs, in

* Corresponding authors at: LNM, Institute of Mechanics, Chinese Academy of Sciences, Beijing 100190, China (C. Wang). Institute of Advanced Structure Technology, Beijing Institute of Technology, Beijing 100081, China (S. Chen).
E-mail addresses: wangchao@lnm.imech.ac.cn (C. Wang), shchen@bit.edu.cn (S. Chen).

https://doi.org/10.1016/j.commatsci.2022.111277
Received 22 September 2021; Received in revised form 10 February 2022; Accepted 13 February 2022
Available online 25 February 2022

which it was found that the microstructures and mechanical properties of GrFs could be althered through shear deformation. Sandeep et al. [28,29] studied the fracture behavior and shockwave response of GrFs using FAMD. They found that the fracture toughness depends powerlawly on the density with an exponent of 1.41 ± 0.04 and obtained a linear relationship between the shock velocity and particle velocity. Using a coarse-grained molecular dynamics (CGMD) model [38], Wang et al. [20,22] systematically studied the microstructure deformation mechanism of GrFs under uniaxial compression and found three major energy dissipation mechanisms, i.e., sliding, impacting and rippling of graphene sheets. Furthermore, they found that the deformation of GrFs is dominated by the bending deformation of flakes instead of the stretching one. Combining the transport modeling with CGMD, Liu et al. [34] studied the critical phenomenon of the maximum conductivity of GrFs and explained the competition mechanism between the conductivity of single graphene sheet and the density of contacting points among sheets. Xia et al.[4] adopted the CG model [39] of graphene sheets to study the temperature-dependent behavior of GrFs and found a fluid-like behavior similar to linear polymer melting at elevated temperatures and the transformation into a glassy-like "foam" state at temperatures below the glass-transition temperature T_g.

All the above studies are on the mechanical properties of pure GrF materials. What are the mechanical properties of GrFs filled with nanoparticles? How does the nanoparticle influence the mechanical properties of NP-GrFs? Experimental results have shown at least two kinds of effects induced by NPs in GrFs. One is the embedded NPs can effectively restrain the aggregation of graphene sheets due to the so-called "spacer effect" [40] to reach a high specific surface area; the other is that the unavoidable aggregation of NPs in GrFs will deteriorate the performance of composites [41]. However, these are far from enough to understand the mechanical properties of this kind of material and the inner microstructure mechanisms. Many questions are not clear, such as how particles interacting with graphene sheets, how particles affecting the self-assembly of microstructure or the distribution of internal energy, how particles affecting the macroscopic properties of NP-GrFs, what difference of all these phenomena under the tensile or compressive loading?

We have preliminarily studied the deformation behavior of NP-GrFs under uniaxial compression [42] and found that the compressive behavior depends seriously on the particle size. Beyond a critically relative particle size, the graphene-sheet-dominated deformation mode would change to be a NP-dominated one. As we know from previous experimental and numerical studies [20,24,36], the deformation behaviors of pure GrFs in tension are much different from that in compression due to the varied microscopic mechanisms of bond breaking and flake deformation. So, what is the mechanical response of NP-GrFs under uniaxial tension? Moreover, the inter-sheet crosslinks may play a key role in maintaining the integrity of foam structures and improving the mechanical performance of GrFs [20,21,33], it can be reasonably inferred that the migration of NPs in a crosslinked GrFs and the effect on the mechanical properties of crosslinked GrFs should be much different from those in pure GrFs.

In this work, the mechanical property and microscopic deformation mechanism of NP-GrFs with crosslinks under uniaxial tension are studied with numerical experiment, in which effects of size and volume fraction of NPs are mainly focused on. First, the numerical model of NP-GrFs enhanced by crosslinking is established. Systematic simulations of NP-GrFs under uniaxial tension are then carried out to find the macroscopic mechanical properties, including the initial elastic behavior, the strain hardening behavior and the final strength. The microscopic mechanism is further analyzed in detail. Conclusions are given finally.

2. Numerical model of NP-GrFs

2.1. Mesoscopic coarse-grained method and parameters

The coarse-grained graphene model [38] that has been well used to study the deformation mechanisms and mechanical properties of both single graphene sheets and pure GrFs [20–22,33,34,43] is adopted in this work. The details of numerical model regarding mesoscopic course-grain method and related parameters of pure GrFs can be found in our previous work [42].

In order to mimic the strong connection among neighboring sheets due to the strong physical crosslinks or chemical functional groups [11,49] in actual GrF systems, based on the numerical model of pure GrFs, we adopt a crosslink model that has been widely used to study the large-deformation behavior and fracture mode of carbon nanotube buckypapers [49,50] and graphene foams [27,46]. As shown in Fig. 1b, a certain amount of crosslinks (red color) characterized by $\phi_C = k_C(r - r_0)^2/2$ are added among neighboring sheets in GrF samples. k_C is the spring constant to mimic the bonds in graphene sheets, r is the current distance between two beads in different sheets with an equilibrium distance r_0 = 25 Å. The initial crosslink density in GrFs is fixed in all simulation models. Furthermore, we assume that the bonds in sheets as well as crosslinks between neighboring sheets will break when the local tensile strain is larger than the critical value of 12% according to the experimental and theoretical researches on the fracture of graphene [51,52].

2.2. Establishment of the numerical model of NP-GrFs

The numerical model of NP-GrF is divided into three steps according to the experimental method [13]: first, a pure GrF without NPs is assembled with 100 square CG sheets (the side length of 50 nm), which are randomly distributed in a box with the length, width and height about 178 nm, 170 nm and 180 nm, respectively. A certain amount of crosslinks are added into the as-synthesized pure GrF to connect neighboring sheets like strong chemical bonds in actual systems [44]; Then, NPs of a certain volume fraction are randomly intercalated into the porous structure of the cross-linked GrF; Finally, an equilibrium simulation is conducted to achieve a well-equilibrated NP-GrF with the total energy fluctuation less than 1% as shown in Fig. S1. The pure GrF density of the numerical model is in the range of ~180 mg/cm^3, which is in line with the density range of 12–280 mg/cm^3 in experiments [45–47]. The density would be changed accordingly with the volume fraction of NPs. In an actual GrF material, the graphene sheet may consist of 1–10 graphene layers [36,48,49]. Here, 8-layered sheets are mainly adopted in this paper and the sheet layer effect on the mechanical response of pure GrFs can be found in [24].

The NPT assembly technique (constant number of atoms, constant pressure and constant temperature) is adopted to deal with the NP-GrF system, which has periodic boundary conditions in all three directions and a constant room temperature of 300 K as well as one barometric pressure. A time step of 1 fs is used. All simulations are performed in the large-scale atomic/molecular massively parallel simulator (LAMMPS) [50] and the results are visualized based on the Open Visualization Tool (OVITO) [51].

Fig. 1a shows the initial state of a well-equilibrated 3D NP-GrF model, in which graphene sheets colored in blue are randomly distributed and bonded by crosslinks as depicted in Fig. 1b. NPs colored in green randomly deposit on graphene sheets in three typical forms as shown in Fig. 1c. It is noted that, the widely observed three structures in experiments [19,52–55], i.e., the randomly-distributed graphene sheets, the crosslink-enhanced connections between neighboring sheets, and the randomly-deposited NPs, are well captured in the numerical model. The mechanical property under uniaxial tension is manly focused on in this work and the uniaxial tension added in the x direction has a strain rate of 5×10^7 s^{-1} along with a zero-pressure barostat in the other two

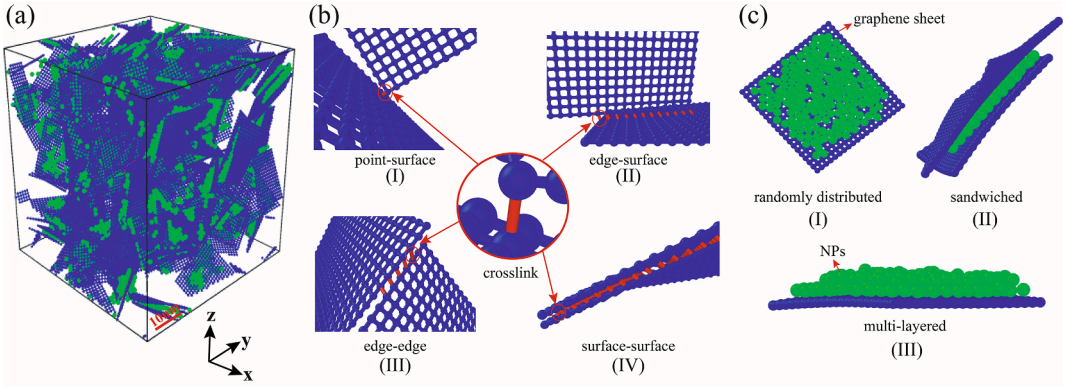

Fig. 1. Numerical model of 3D NP-GrFs. (a) The initial well-equilibriated configuration of a NP-GrF with NPs (green) adsorbed on graphene sheets (blue); (b) Four typical crosslinked microstructures: b-I. point-surface; b-II. edge-surface; b-III. edge-edge and b-IV. surface-surface; (c) Three typical NP-sheet microstructures: c-I. single-layer NPs randomly adsorbed on a graphene sheet; c-II. NPs sandwiched between two graphene sheets and c-III. multi-layers NPs on a graphene sheet.

loading-free directions. In order to eliminate the influence of graphene foams and extract the effect of nanoparticles as much as possible, for a given particle size and volume fraction, we produce the three numerical samples with the same configuration of graphene foams but different distribution of nanoparticles in foams to study the effect of the two factors.

3. Size effect of NPs on the mechanical property and its micro-mechanism

The tensile stress-strain curves of NP-GrFs with varied NP sizes, i.e., $D = 7\%$, 26% and 50% for a constant volume fraction $v_f = 2\%$ of NPs are given in Fig. 2a. Here, $D = d/L$, where d and L denote the diameter of NPs and the side length of square graphene sheets, respectively. The stress-strain relation of the NP-GrF with a volume fraction $v_f = 2\%$ of NPs has a similar trend as that of pure GrFs in experiment [36] and simulation [20]. The stress increases sharply in the initial elastic stage before reaching a maximum value at a relatively low strain, then decreases slightly with an increasing tensile strain due to the gradual breakage of different connections and rearrgement of microstrucutres. As indicated by the green curve for the NP-GrF with $D = 26\%$, the bond breaking occurs as early as the tensile strain reaches about 0.1 and the number of broken bonds continues to increase during the subsequent tension process. Four successive snapshots of the system with $D = 26\%$ at the tensile strain $\varepsilon = 0$, 0.2, 0.4 and 0.6 are shown in Fig. 2b for an intuitive description of tension process.

An interesting finding is that the mechanical response is greatly influenced by the size of NPs as shown in Fig. 2a. The initial modulus of the stress-strain relation increases with the increasing NP size when the volume fraction of NPs is fixed as shown in Fig. 2c. Such a phenomenon is opposite to that in the other particle-filled composites [59]. In the present material, the initial modulus increases almost linearly with D in the range of $0 < D < 15\%$ and then nonlinearly in the range of $15\% < D < 50\%$; Afterwards, it keeps nearly a constant when $D > 50\%$. Furthermore, the initial modulus increases almost an order of magnitude when the relative size D increases from 0 to 50%. Here, we noted that this relationship between the initial modulus and particle size in the NP-GrFs under uniaxial tension is highly different from that observed in

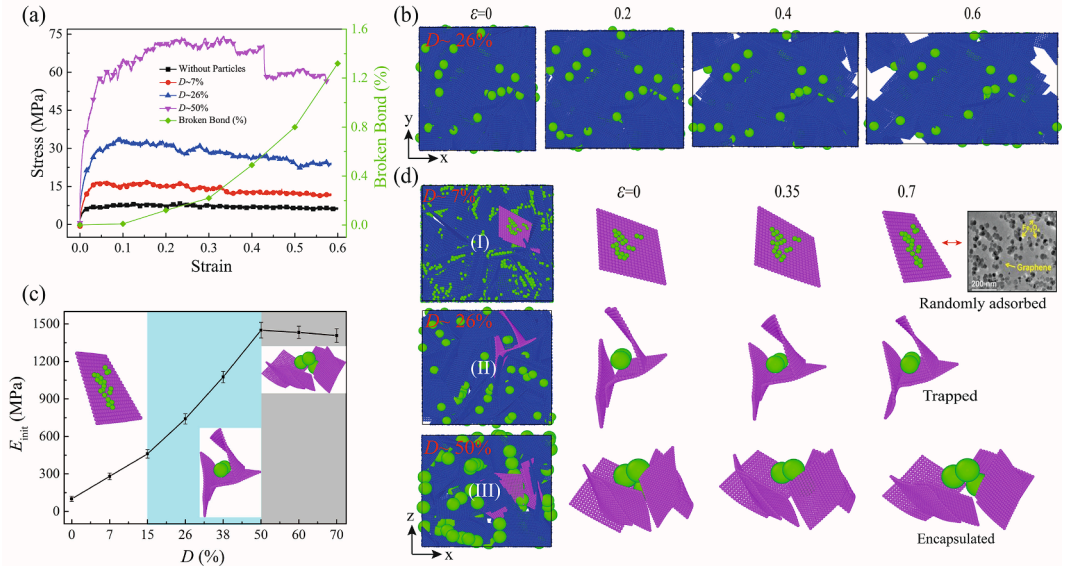

Fig. 2. Mechanical responses of NP-GrFs with a varied NP size under uniaxial tension. (a) The stress and the percentage of broken bonds as a function of the tensile strain for the system with varied relative particle diameters $D = 7\%$, 26% and 50% at a given volume fraction of NPs $v_f = 2\%$. The percentage of broken bonds is the number of broken bonds divided by the total number of bonds in the system; (b) Snapshots of the NP-GrFs with $D = 26\%$ at four successive tensile strains of 0, 0.2, 0.4 and 0.6; (c) The modulus of NP-GrFs as a function of D; (d) Microstructural evolution in NP-GrFs with varied $D = 7\%$, 26% and 50%, (d-I) Small particles with $D = 7\%$ are randomly adsorbed on sheets similar to that in experiment [19]; (d-II) Medium particles with D = 26% are trapped between crosslinked neighboring sheets; (d-III) Large NPs with $D = 50\%$ are encapsulated in pores surrounded by multiple crosslinked sheets.

uniaxial compression [42].

In order to reveal the mechanism of size-dependent initial modulus, the evolution of microstructures are given in Fig. 2d. As observed in experiments [19,56], NPs of $D \leq 15\%$ adhere randomly on the graphene sheet and have hardly effect on the rearrangement of graphene sheets in the tension process of NP-GrFs as shown in Fig. 2d-I. However, according to the numerical calculation [57], the modulus of a single graphene sheet can be well enhanced by other coating materials, such as CNTs, graphene sheets or NPs, which will further increase the modulus of GrFs. In the case of relatively large NPs, i.e., $15\% < D \leq 50\%$, NPs aggregate at junctions between two neighboring crosslinked graphene sheets due to the greater interaction. The case of $D = 26\%$, as an example, is shown in Fig. 2d-II, where it is found that the "trapped" NPs will constrain the relative rotation of graphene sheets and trigger not only larger out-of-plane bending deformation of sheets, but also larger in-plane stretching deformation. Such a microstructural phenomenon will be further verified by the energy analysis in the following part. Both the increased stretching modulus and the bending modulus of graphene sheets should be responsible for the enhanced modulus of NP-GrFs. In the case of $D > 0.50$, nanoparticles cannot be trapped by neighboring bonded sheets due to the narrow space, which will drift into pores and be surrounded by bonded sheets as an "encapsulated" configuration shown in Fig. 2d-III. Such a configuration can increase the interaction among distant sheets and restrain their rearrangement, which further induces a large modulus of the system. However, it can be inferred that the effects of increasing interaction and restraining rearrangement tends to be saturated with the further increase of nanoparticles, which is also verified by the final stage in the results of Fig. 2c. Movies M1, M2 and M3 for the three configurations of NPs in GrFs are supplied in Supplementary Materials. In our previous work [42] studying the compression of NP-GrFs, the NP size also had direct influence on the stress-strain behavior of NP-GrFs due to different micromechanism. In uniaxial compression, the large particles can flow out and agglomerate to form a skeleton to support the external load, in this case, the compressive modulus of NP-GrFs is dominated by large NPs rather than graphene sheets.

One should be noted that, the relationship between the modulus of NP-GrFs and the size of NPs is opposite to that in other particle-modulated composites [58,59]. For example, in nanoscale $CaCO_3$ and silica particles filled polypropylene and polysiloxane matrices, the modulus of the composite decreases with an increasing size of particles when the volume fraction of nanoparticles is fixed. Such a result is mainly due to the reduced interface between nanoparticles and matrix. In addition, in real applications, NPs may damage the GrF structures to some extent, e.g., leading to thinner pore walls or less inter-sheet crosslinking, as mentioned in Fe_3O_4 filled GrFs [19]. As a result, the modulus of the composite would be decreased by nanoparticles. In comparison, the present result indicates that, it is an effective way to tune or increase the initial modulus of GrFs by the size of nanoaprticles with a fixed volume fraction, only if the foam structure is not damaged during in the fabrication process.

In order to further reveal the micro-mechanism of size-dependent initial modulus, we study the distribution and evolution of three kinds of elastic energies, i.e., the bending energy U_{bend}, the stretching energy $U_{stretch}$ and the shear deformation energy U_{shear} of graphene sheets, respectively, as shown in Fig. 3 (a-c). In any system, both the bending energy U_{bend} and the stretching one $U_{stretch}$ are much larger than the shear deformation energy U_{shear} at any tensile strain. It indicates that the bending and stretching behaviors are dominated in the deformation of NP-GrFs under tension, which is much similar to that in pure GrFs [20]. Furthermore, it is found that the larger the nanoparticle, the larger U_{bend}, $U_{stretch}$ and U_{shear} will be in the NP-GrFs. All these are consistent well with the qualitative description and observations in Fig. 2d(II and III). In addition, in the system without NPs or with smaller NPs ($D =$

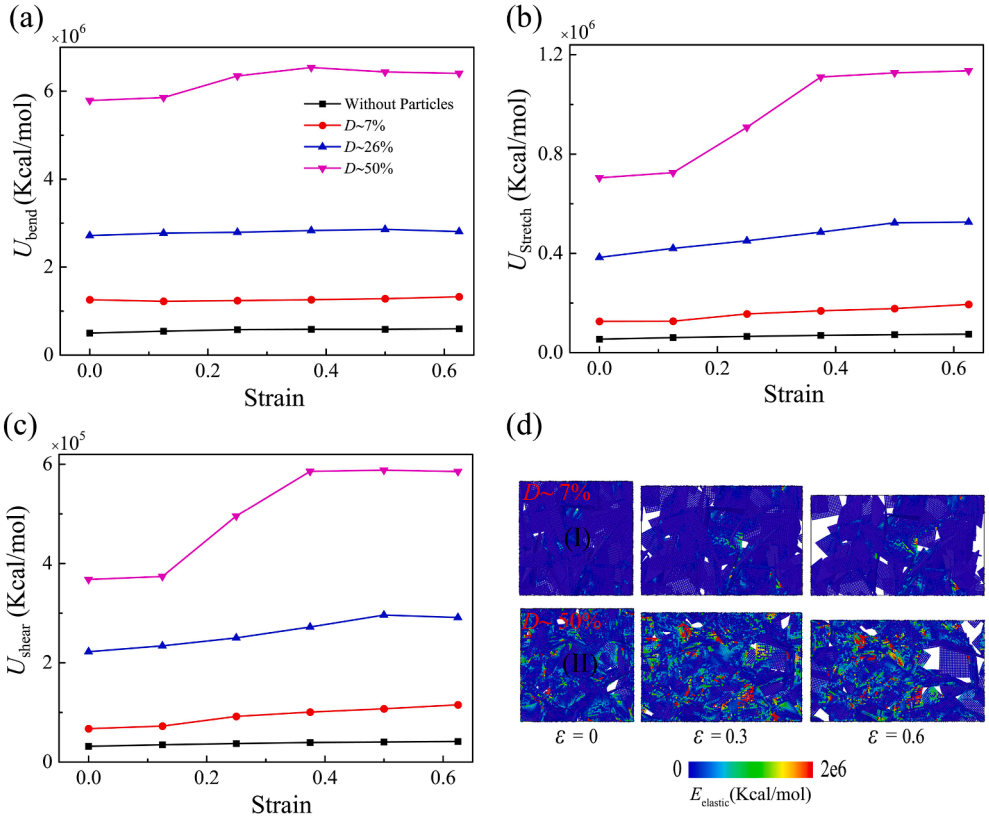

Fig. 3. The distribution and evolution of different elastic energies in NP-GrFs with varied D under uniaxial tension. (a) The bending energy U_{bend}; (b) The stretching energy $U_{stretch}$ and (c) the shear deformation energy U_{shear}; (d) Snapshots of the total elastic energy at the initial state and the states with 0.3 and 0.6 tensile strain in NP-GrFs with different D: (d-I) 7% and (d-II) 50%.

7%), U_{bend}, $U_{stretch}$ and U_{shear} increase negligibly with an increasing tensile strain, while in the system with larger NPs (e.g., D = 26% or 50%), three kinds of energies, especially the stretching one $U_{stretch}$, increase obviously with an increasing tensile strain due to the constraint effect of NPs. Compared the total elastic energy in NP-GrF of D = 7% with that of D = 50%, as shown in Fig. 3d, shows that the larger the NPs, the more uneven the high elastic energy regions will be.

4. The effect of volume fraction of NPs on the mechanical property and its micro-mechanism

The effect of volume fraction of NPs on the mechanical properties of NP-GrFs is further studied. Considering the widely used small NPs in practical applications, we adopt nanoparticles of D = 7% in this subsection. The stress-strain relations of NP-GrFs with varied volume fractions of NPs v_f = 2%, 16%, 30% and 42% are shown in Fig. 4a. Basically, the stress-strain relation is similar to that of pure GrFs. However, the stress-strain relation exhbites an obvious strain hardening effect with the increasing volume fraction, especially, in the case with v_f = 30% and 42%. Four successive snapshots of GrF with v_f = 42% under the tensile strain of 0, 0.2, 0.4 and 0.65 are given in Fig. 4b. It can be seen that NPs almost fill the entire foam system. With the increase of tension, microcrack or hole emerges and grows up in the cluster of nanoparticles. Then, the crack or hole is blocked by the graphene sheets and stops the further growth. Cracks or holes will appear in other NP clusters at other locations, which will grow up and be blocked also by the graphene sheets. This phenomenon occurs repeatedly and multiple microcracks form in different places, which is the main micro- mechanism inducing the effect of strain hardening. The larger the volume fraction of NPs, the more the number of final microcracks will be, and the more obvious the strain hardening effect will be.

Fig. 4a further shows that the initial modulus and final strength of NP-GrFs are also influenced by the volume fraction of NPs as shown in Fig. 4c. The molulus increases almost linearly with an increasing v_f, which can be fitted by a formula $E_{init} = 192v_f\text{-}114$. Here, we noted that this dependency relationship of the modulus on the volume fraction of NPs is much different from that in compression [42], in which a maximum initial modulus is obtained at a critical volume fraction of NPs. The strength exhibits an exponential relation with v_f, which nearly abides by $\sigma_T = 7.1 + 2.9\exp(0.6v_f\text{-}0.5)$.

Two micro-mechanisms may be responsible for the increased modulus of NP-GrFs. One is the increased effective modulus of graphene sheet due to the adsorbed NPs in the case of small v_f, the discussion on which is the same as that in Section 3.1. The other is the constraint effect in the case of large v_f, in which the elastic deformation of graphene sheets themselves is activated due to the particle constraints. Further analysis from the deformation energy point of view will be given later. Generally, the micro-mechanism for the emhancing modulus of NP-GrFs with varied v_f is similar to that with varied particle size in Section 3.

The increased strength of NP-GrFs may attributes to two micro-mechanisms. One is the connecting effect induced by NPs, which look like glue between neighboring sheets as shown in Fig. 5a and movie M4 in Supplementary Materials. The more the NPs, the more obvious such a connecting effect will be. The other is due to the strain hardening effect induced by microcracks or holes, especially in the case with large volume fraction. The larger the volume fraction of NPs, the more microcracks or holes will be formed. On the one hand, the blocking effect by the graphene sheet will increase the strength. On the other hand, more cracks or holes are conducive to more dispersed distribution of high stress zone as shown in Fig. 5b, which will further reduce the number of broken bonds as shown in Fig. 5c.

Different elastic energies of graphene sheets in NP-GrFs with v_f = 0, 2%, 16% and 42%, including the bending energy, the shearing deformation energy and the stretching energy, are calculated and shown in Fig. 6(a-c). Generally, the three kinds of elastic energies increase with an increasing v_f. Specially, in the system with nanoparticles of large volume fraction, the deformation of graphene sheets may be relatively large, which can be inferred from the elastic energies shown in Fig. 6(a-c). Typical snapshots are given in Fig. 6d, in which the graphene sheet in the system with v_f = 42% bends much more obviously than that in the system with v_f = 16% at the same tensile strain of 0.3. One should note that crosslinks among graphene sheets play a key role in such a mechanical response of NP-GrFs with large v_f. The strong restriction induced by crosslinks causes graphene sheets undergo a relatively large deformation. Without crosslinks [42], the modulus would increase first and then decrease with an increasing volume fraction of NPs.

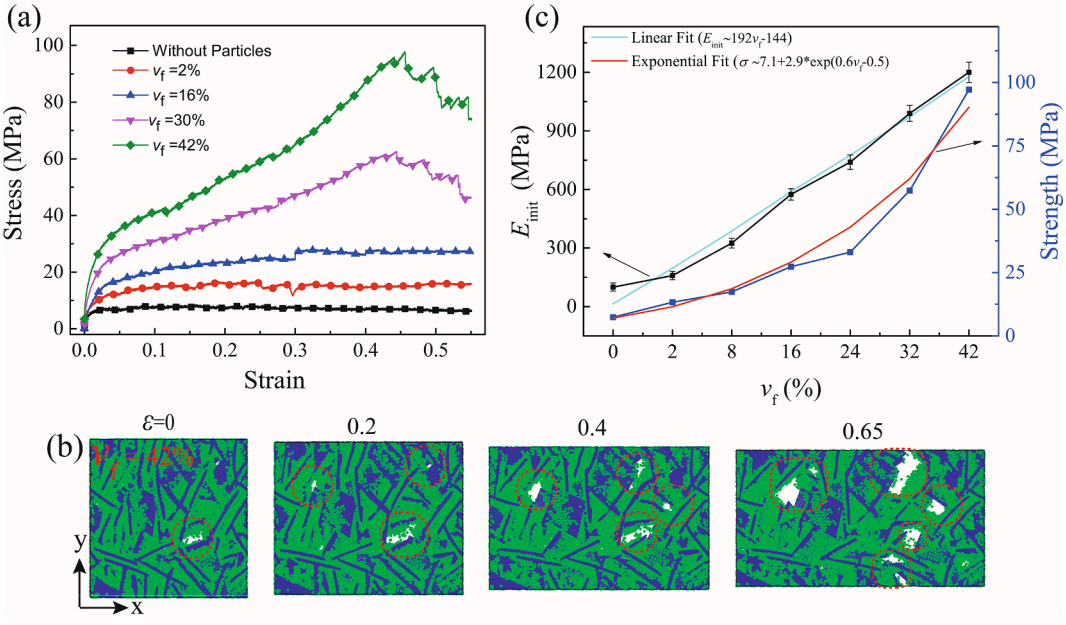

Fig. 4. Effect of the volume fraction of NPs on the mechanical properties of NP-GrFs under uniaxial tension. (a) The stress-strain relation of NP-GrFs with varied volume fractions: v_f = 0, 2%, 16%, 30% and 42%; (b) Snapshot at the tensile strain of 0, 0.2, 0.4 and 0.65 in NP-GrF with v_f = 42%; (c) The modulus and strength of NP-GrFs as a function of v_f as well as their respective fitting curves.

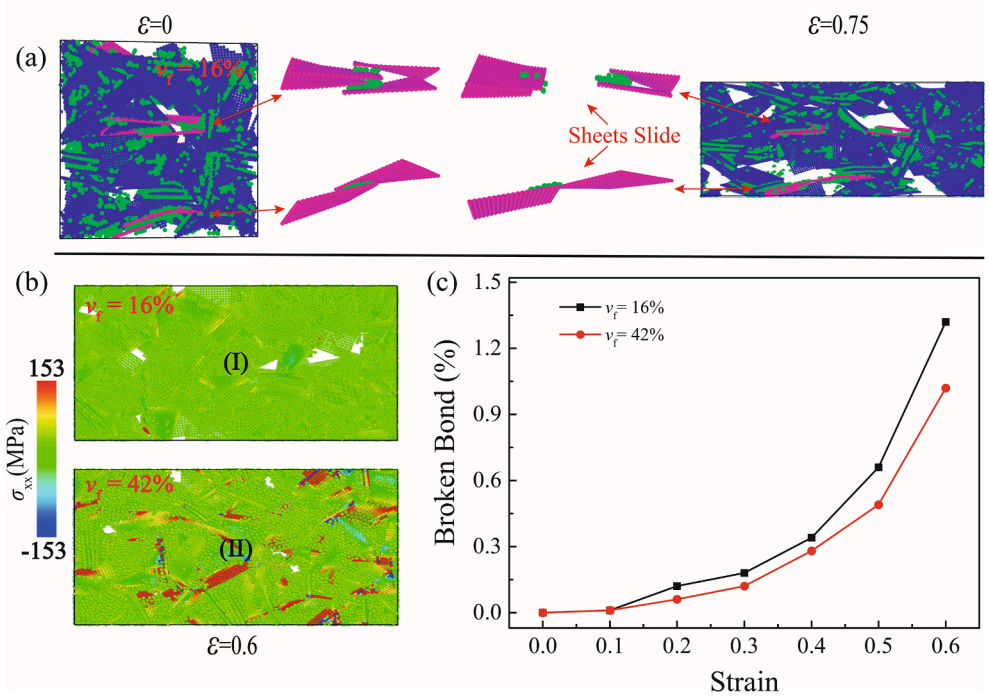

Fig. 5. The micro-mechanisms of the enhanced strength of NP-GrFs with varied v_f under uniaxial tension. (a) NPs enhance the connection between graphene sheets like glue; (b) The distribution of virial stress σ_{xx} in the tension direction in NP-GrFs with $v_f = 16\%$ and 42% at the strain of 0.6; (c) The percentage of broken bonds in NP-GrFs with $v_f = 16\%$ and 42% as a function of tensile strain.

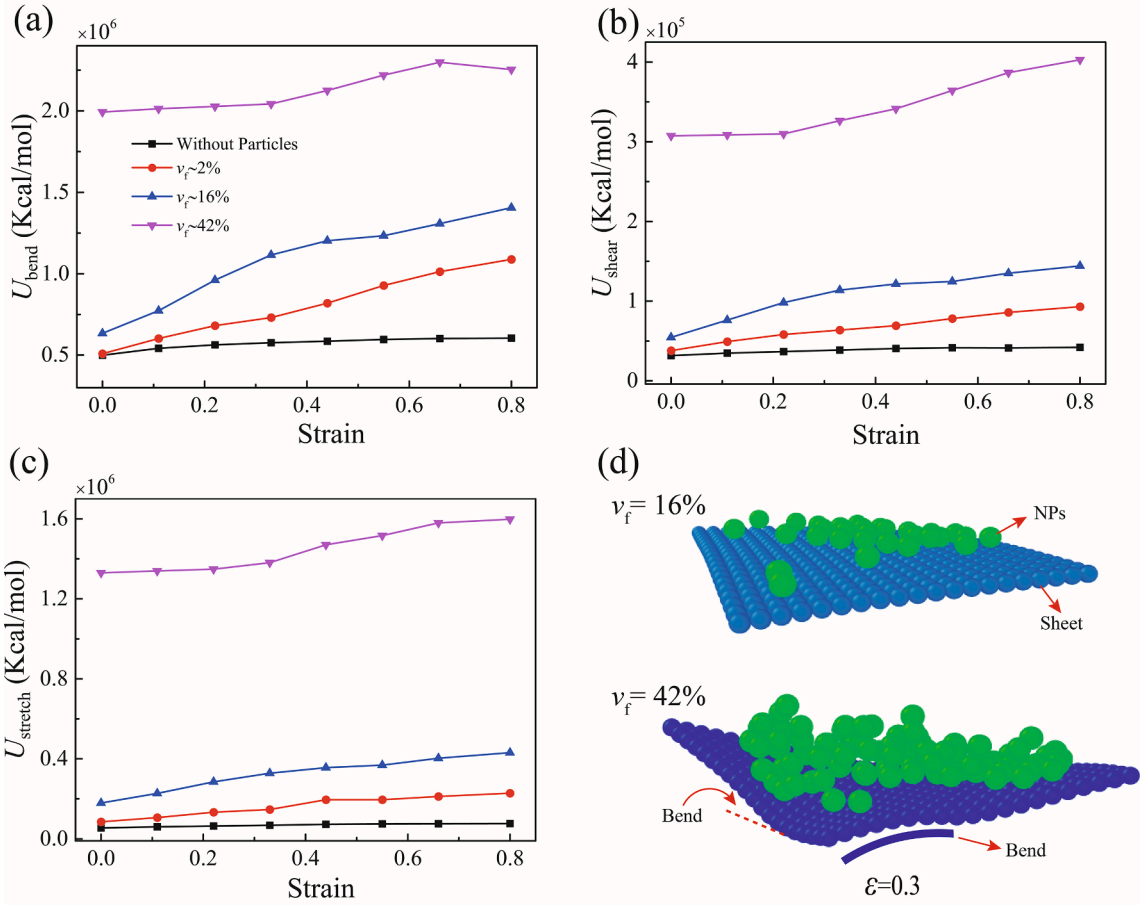

Fig. 6. The distribution and evolution of different elastic energies in NP-GrFs with varied volume fractions v_f under uniaxial tension. (a) The bending energy U_{bend}; (b) The shear deformation energy U_{shear} and (c) the stretching energy $U_{strectch}$; (d) The deformation of graphene sheet in NP-GrFs with $v_f = 16\%$ and 42%.

5. Conclusion

In this work, the mechanical property and the corresponding microscopic deformation mechanism of NP-GrFs under uniaxial tension are systematically investigated using the CGMD method. The effects of size and volume fraction of NPs on the stress-strain relationship and microstructural evolution are mainly focused on. It is found that, with the increase of NP size, NP-GrFs have three kinds of microstructures, i.e., NPs randomly adsorbed on sheets, trapped between two neighboring crosslinked sheets and encapsulated in pores formed by interconnected sheets. The initial modulus of NP-GrFs depends nonlinearly on the particle size and increases by almost an order of magnitude as the relative size D increasing from 2% to 50%. For the system with smaller NPs ($0 < D < 15\%$), the increase of modulus is attributed to the enhanced constituent sheets by NPs; while for the system with larger NPs ($15\% < D < 50\%$), besides of the enhancing effect of constituent sheets, NPs will restrain the rearrangement of sheets and trigger large deformation of sheets, which is responsible for the further increase of the modulus of the system. Distribution and evolution of three kinds of elastic deformation energies in sheets further provide quantitatively explaination on the relationship between the modulus and particle size. The volume fraction of NPs has also significant effect on the modulus and strength of NP-GrFs. The initial modulus increases almost linearly with an increasing volume fraction of NPs, the micromechanism is much similar to that induced size-dependent initial modulus. The strength of the system increases nearly exponentially with an increasing volume fraction of NPs due to two underlying mechanisms: one is the enhanced adhesion by NPs between two neighboring sheets and the other is the homogenization of stress due to the gradually formed microcracks in the case with large volume fraction of NPs. The results in this work should be useful not only for understanding the microstructure-determined mechanical properties of NP-GrFs but also for the design of advanced functional materials or devices based on GrFs.

CRediT authorship contribution statement

Muhammad Bilal Khan: Methodology, Software, Validation, Formal analysis, Investigation, Data curation, Writing – original draft, Supervision. **Chao Wang:** Conceptualization, Methodology, Writing – review & editing, Validation, Supervision, Project administration. **Shuai Wang:** Writing – review & editing. **Shaohua Chen:** Conceptualization, Resources, Writing – review & editing, Visualization, Supervision, Project administration, Funding acquisition.

Declaration of Competing Interest

The authors declare no competing interests. The authors declare that they have no known competing financial interests or personal relationships that could have appeared to influence the work reported in this paper.

Acknowledgements

The work reported here is supported by NSFC through Grants #11872114, #12032004, #11972348, #12002034, Strategic Priority Research Program of the Chinese Academy of Sciences (Grants No. XDB22040503) and the CAS/SAFEA International Partnership Program for Creative Research Teams.

Data availability

The raw/processed data required to reproduce these findings cannot be shared at this time as the data also forms part of an ongoing study.

Appendix A. Supplementary material

Supplementary data to this article can be found online at https://doi.org/10.1016/j.commatsci.2022.111277.

References

[1] L. Qiu, B. Huang, Z. He, Y. Wang, Z. Tian, J.Z. Liu, K. Wang, J. Song, T. R. Gengenbach, D. Li, Extremely Low Density and Super-Compressible Graphene Cellular Materials, Adv. Mater. 29 (36) (2017) 1701553.
[2] Y. Tao, et al., Towards ultrahigh volumetric capacitance: graphene derived highly dense but porous carbons for supercapacitors, Sci. Rep. 3 (2013) 2975.
[3] Y. Wu, et al., Three-dimensionally bonded spongy graphene material with super compressive elasticity and near-zero Poisson's ratio, Nat. Commun. 6 (2015) 6141.
[4] W. Xia, F. Vargas-Lara, S. Keten, J.F. Douglas, Structure and dynamics of a graphene melt, ACS Nano 12 (6) (2018) 5427–5435.
[5] S.M. Lyth, H. Shao, J. Liu, K. Sasaki, E. Akiba, Hydrogen adsorption on graphene foam synthesized by combustion of sodium ethoxide, Hydrogen Energy 39 (1) (2014) 376–380.
[6] L. Yi, T. Chang, X.-Q. Feng, Y. Zhang, J.i. Wang, B. Huang, Giant energy absorption capacity of graphene-based carbon honeycombs, Carbon 118 (2017) 348–357.
[7] H. Zhao, X. Song, H. Zeng, 3D white graphene foam scavengers: vesicant-assisted foaming boosts the gram-level yield and forms hierarchical pores for superstrong pollutant removal applications, NPG Asia Mater. 7 (3) (2015) e168.
[8] Z. Jiao, et al., Combining carbon nanotube foam with nanosilver/silicone resin or graphene foam for advanced metamaterial design, Mater. Sci. 55 (34) (2020) 16211–16219.
[9] A. Nieto, et al., Three dimensional graphene foam/polymer hybrid as a high strength biocompatible scaffold, Adv. Funct. Mater. 25 (25) (2015) 3916–3924.
[10] Y. Chen, G. Dai, Q. Gao, Starch Nanoparticles-Graphene Aerogels with High Supercapacitor Performance and Efficient Adsorption, ACS Sustainable Chem. Eng. 7 (16) (2019) 14064–14073.
[11] B. Zhao, T. Sun, X.i. Zhou, X. Liu, X. Li, K. Zhou, L. Dong, D. Wei, Three-Dimensional Graphene Composite Containing Graphene-SiO_2 Nanoballs and Its Potential Application in Stress Sensors, Nanomaterials 9 (3) (2019) 438, https://doi.org/10.3390/nano9030438.
[12] B. Qiu, M. Xing, J. Zhang, Mesoporous TiO_2 nanocrystals grown in situ on graphene aerogels for high photocatalysis and lithium-ion batteries, Am. Chem. Soc. 136 (16) (2014) 5852–5855.
[13] Y. Wang, et al., Fe_3O_4 nanoparticle/graphene aerogel composite with enhanced lithium storage performance, App. Surf. Sci. 458 (2018) 1035–1042.
[14] E. Pan, et al., Facile synthesis of mesoporous 3D CoO/nitrogen-doped graphene aerogel as high-performance anode materials for lithium storage, Micr. Meso. Mater. 267 (2018) 93–99.
[15] L. Li, S. He, M. Liu, C. Zhang, W. Chen, Three-dimensional mesoporous graphene aerogel-supported SnO_2 nanocrystals for high-performance NO_2 gas sensing at low temperature, Analy. Chem. 87 (3) (2015) 1638–1645.
[16] C. Shen, E. Barrios, M. McInnis, J. Zuyus, L. Zhai, Fabrication of graphene aerogels with heavily loaded metallic nanoparticles, Micromachines 8 (2) (2017) 47, https://doi.org/10.3390/mi8020047.
[17] Z. Juanjuan, L.i. Ruiyi, L.i. Zaijun, L. Junkang, G.u. Zhiguo, W. Guangli, Synthesis of nitrogen-doped activated graphene aerogel/gold nanoparticles and its application for electrochemical detection of hydroquinone and o-dihydroxybenzene, Nanoscale 6 (10) (2014) 5458–5466.
[18] X. Liu, et al., 3D graphene aerogel-supported SnO_2 nanoparticles for efficient detection of NO_2, RSC. Adv. 4 (43) (2014) 22601–22605.
[19] X. Xu, H. Li, Q. Zhang, H. Hu, Z. Zhao, J. Li, J. Li, Y.u. Qiao, Y. Gogotsi, Self-sensing, ultralight, and conductive 3D graphene/iron oxide aerogel elastomer deformable in a magnetic field, ACS Nano 9 (4) (2015) 3969–3977.
[20] C. Wang, C. Zhang, S. Chen, Micro-mechanism and influencing factors of graphene foam elasticity, Carbon 148 (2019) 267–276.
[21] D. Pan, C. Wang, X. Wang, Graphene Foam: Hole-Flake Network for Uniaxial Supercompression and Recovery Behavior, ACS Nano 12 (11) (2018) 11491–11502.
[22] C. Wang, D. Pan, S. Chen, Energy dissipative mechanism of graphene foam materials, Carbon 132 (2018) 641–650.
[23] P. Nautiyal, B. Boesl, A. Agarwal, Harnessing Three Dimensional Anatomy of Graphene Foam to Induce Superior Damping in Hierarchical Polyimide Nanostructures, Small 13 (10) (2017) 1603473, https://doi.org/10.1002/smll.v13.1010.1002/smll.201603473.
[24] C. Wang, C. Zhang, S. Chen, The microscopic deformation mechanism of 3D graphene foam materials under uniaxial compression, Carbon 109 (2016) 666–672.
[25] L. Qiu et al., Biomimetic superelastic graphene-based cellular monoliths 3(1) (2012) 1–7.
[26] Z. Qin, G.S. Jung, M.J. Kang, M.J. Buehler, The mechanics and design of a lightweight three-dimensional graphene assembly, Sci. Adv. 3 (1) (2017), https://doi.org/10.1126/sciadv.1601536.
[27] J.A. Baimova, L.K. Rysaeva, B.o. Liu, S.V. Dmitriev, K. Zhou, From flat graphene to bulk carbon nanostructures, Phys. Status Solidi B-Basic Solid State Phys. 252 (7) (2015) 1502–1507.
[28] S.P. Patil, A. Kulkarni, B. Markert, Shockwave response of graphene aerogels: An all-atom simulation study, Comput. Mater. Sci. 189 (2021), 110252.

[29] S.P. Patil, P. Shendye, B. Markert, Molecular investigation of mechanical properties and fracture behavior of graphene aerogel, Phys. Chem. B 124 (28) (2020) 6132–6139.
[30] G.S. Jung, M.J. Buehler, Multiscale mechanics of triply periodic minimal surfaces of three-dimensional graphene foams, Nano Lett 18 (8) (2018) 4845–4853.
[31] W. Gao, et al., Effect of flake size on the mechanical properties of graphene aerogels prepared by freeze casting, RSC. Adv. 7 (53) (2017) 33600–33605.
[32] X. Zhang, et al., Theoretical strength and rubber-like behaviour in micro-sized pyrolytic carbon, Nat. Nanotech. 14 (8) (2019) 762–769.
[33] D. Pan, C. Wang, T.-C. Wang, Y. Yao, Graphene foam: uniaxial tension behavior and fracture mode based on a mesoscopic model, ACS Nano 11 (9) (2017) 8988–8997.
[34] F. Liu, C. Wang, Q. Tang, Conductivity maximum in 3D graphene foams, Small 14 (32) (2018) 1801458, https://doi.org/10.1002/smll.v14.3210.1002/smll.201801458.
[35] L. Rizzi, A. Zienert, J. Schuster, M. Köhne, S.E. Schulz, Electrical conductivity modeling of graphene-based conductor materials, ACS Mater. Sci. 10 (49) (2018) 43088–43094.
[36] A. Nieto, B. Boesl, A. Agarwal, Multi-scale intrinsic deformation mechanisms of 3D graphene foam, Carbon 85 (2015) 299–308.
[37] A. Baimova, et al., Review on crumpled graphene: unique mechanical properties, Rev. Adv. Mat. Sci. 39 (1) (2014) 69–83.
[38] S. Cranford, M.J. Buehler, Twisted and coiled ultralong multilayer graphene ribbons, Modelling Simul. Mater. Sci. Eng. 19 (5) (2011) 054003, https://doi.org/10.1088/0965-0393/19/5/054003.
[39] L. Ruiz, W. Xia, Z. Meng, S. Keten, A coarse-grained model for the mechanical behavior of multi-layer graphene, Carbon 82 (2015) 103–115.
[40] W. Chen, et al., Self-assembly and embedding of nanoparticles by in situ reduced graphene for preparation of a 3D graphene/nanoparticle aerogel, Adv. Mater. 23 (47) (2011) 5679–5683.
[41] K. Chrissafis, K.M. Paraskevopoulos, I. Tsiaoussis, D. Bikiaris, Comparative study of the effect of different nanoparticles on the mechanical properties, permeability, and thermal degradation mechanism of HDPE, Appl. Polym. Sci. 114 (3) (2009) 1606–1618.
[42] M.B. Khan, C. Wang, S. Wang, D. Fang, S. Chen, The mechanical property and microscopic deformation mechanism of nanoparticle-contained graphene foam materials under uniaxial compression, Nanotechnology 32 (11) (2021) 115701, https://doi.org/10.1088/1361-6528/abcfe8.
[43] J. Shang, Q.-S. Yang, X. Liu, C. Wang, Compressive deformation mechanism of honeycomb-like graphene aerogels, Carbon 134 (2018) 398–410.
[44] X. Chen, D. Lai, B. Yuan, M.-L. Fu, Fabrication of superelastic and highly conductive graphene aerogels by precisely "unlocking" the oxygenated groups on graphene oxide sheets, Carbon 162 (2020) 552–561.
[45] W. Kang, Y. Cui, L. Qin, Y. Yang, Z. Zhao, X. Wang, X. Liu, A novel robust adsorbent for efficient oil/water separation: Magnetic carbon nanospheres/graphene composite aerogel, Hazard. Mater. 392 (2020) 122499, https://doi.org/10.1016/j.jhazmat.2020.122499.
[46] Y. Shi, X. Gao, J. Qiu, Synthesis and strengthened microwave absorption properties of three-dimensional porous Fe3O4/graphene composite foam, Ceram. Int. 45 (3) (2019) 3126–3132.
[47] J. Li, S. Yang, P. Jiao, Q. Peng, W. Yin, Y.e. Yuan, H. Lu, X. He, Y. Li, Three-dimensional macroassembly of hybrid C@CoFe nanoparticles/reduced graphene oxide nanosheets towards multifunctional foam, Carbon 157 (2020) 427–436.
[48] Z. Chen, W. Ren, L. Gao, B. Liu, S. Pei, H.-M. Cheng, Three-dimensional flexible and conductive interconnected graphene networks grown by chemical vapour deposition, Nat. Mater. 10 (6) (2011) 424–428.
[49] M. Dienwiebel, G.S. Verhoeven, N. Pradeep, J.W.M. Frenken, J.A. Heimberg, H. W. Zandbergen, Superlubricity of Graphite, Phy. Rev. Lett. 92 (12) (2004), https://doi.org/10.1103/PhysRevLett.92.126101.
[50] S. Plimpton, Fast parallel algorithms for short–range molecular dynamics, J. Comput. Phys. 117 (1) (1995) 1–19.
[51] A. Stukowski, Visualization and analysis of atomistic simulation data with OVITO–the Open Visualization Tool, Modell. Simul. Mater. Sci. Eng. 18 (1) (2010) 015012, https://doi.org/10.1088/0965-0393/18/1/015012.
[52] S. Gu, A. Zhu, Graphene nanosheets loaded Fe_3O_4 nanoparticles as a promising anode material for lithium ion batteries, Alloys Comp. 813 (2020), 152160.
[53] X. Wang, et al., CoFe2O4/N-doped reduced graphene oxide aerogels for high-performance microwave absorption, Chem. Eng. 388 (2020), 124317.
[54] Y. Zhang, N.a. Li, Y. Xiang, D. Wang, P. Zhang, Y. Wang, S. Lu, R. Xu, J. Zhao, A flexible non-enzymatic glucose sensor based on copper nanoparticles anchored on laser-induced graphene, Carbon 156 (2020) 506–513.
[55] H. Yuan, F. Qi, N. Zhao, P. Wan, B. Zhang, H. Xiong, B. Liao, X. Ouyang, Graphene oxide decorated with titanium nanoparticles to reinforce the anti-corrosion performance of epoxy coating, Coatings 10 (2) (2020) 129, https://doi.org/10.3390/coatings10020129.
[56] W. Fan, W. Gao, C. Zhang, W.W. Tjiu, J. Pan, T. Liu, Hybridization of graphene sheets and carbon-coated Fe_3O_4 nanoparticles as a synergistic adsorbent of organic dyes, Mater. Chem. 22 (48) (2012) 25108, https://doi.org/10.1039/c2jm35609k.
[57] S. Wang, C. Wang, M.B. Khan, S. Chen, Microscopic Deformation Mechanism and Main Influencing Factors of Carbon Nanotube Coated Graphene Foams Under Uniaxial Compression, Nanotechnology 32 (34) (2021) 345704, https://doi.org/10.1088/1361-6528/ac020c.
[58] S. Mishra, S. Sonawane, R. Singh, Studies on characterization of nano $CaCO_3$ prepared by the in situ deposition technique and its application in PP-nano $CaCO_3$ composites, Polymer Sci. Part B: Poly. Phys. 43 (1) (2005) 107–113.
[59] J. Douce, J.-P. Boilot, J. Biteau, L. Scodellaro, A. Jimenez, Effect of filler size and surface condition of nano-sized silica particles in polysiloxane coatings, Thin Solid Films 466 (1-2) (2004) 114–122.